

## Supplemental Data

### **Influence of temperature-induced A-site cations redistribution on the functional properties of A-site complex polar perovskite $K_{1/2}Bi_{1/2}TiO_3$**

Gina E Eyoun<sup>1</sup>, Udo Eckstein<sup>1</sup>, Hana Ursic<sup>2,3</sup>, Monica P. Salazar<sup>4</sup>, Gerd Buntkowsky<sup>4</sup>, Pedro B. Groszewicz<sup>5</sup>, Stefano Checchia<sup>6</sup>, Kyle G Webber<sup>1</sup>, Neamul H Khansur<sup>1,\*</sup>

<sup>1</sup>*Department of Materials Science and Engineering, Friedrich-Alexander-Universität Erlangen-Nürnberg, 91058 Erlangen, Germany*

<sup>2</sup>*Electronic Ceramics Department, Jožef Stefan Institute, Ljubljana, Slovenia*

<sup>3</sup>*Jožef Stefan International Postgraduate School, Jamova cesta 39, Ljubljana, Slovenia*

<sup>4</sup>*Institute of Physical Chemistry, Technische Universität Darmstadt, 64287, Darmstadt, Germany*

<sup>5</sup>*Department of Radiation Science and Technology, Delft University of Technology, Delft 2629JB, Netherlands*

<sup>6</sup>*ESRF, The European Synchrotron, 71 Avenue des Martyrs, CS40220, 38043 Grenoble Cedex 9, France*

*\*corresponding author: neamul.khansur@fau.de*

## 1. Temperature-dependent dielectric permittivity for samples cooled with different cooling rates from the T<sub>max</sub> of 900 °C

Temperature-dependent dielectric permittivity measured up to 600 °C during heating for KBT samples cooled with different cooling rates from the T<sub>max</sub> of 900 °C. The room temperature permittivity value increases with decreasing cooling rate.

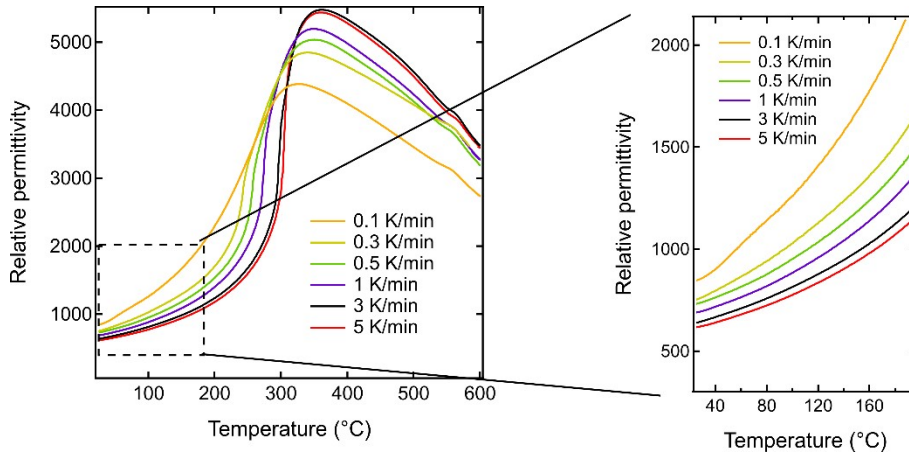


Figure S 1 Temperature-dependent dielectric permittivity of KBT samples treated with different cooling rates from the T<sub>max</sub> of 900 °C.

## 2. Temperature-dependent dielectric permittivity of slow-cooled KBT from different $T_{\text{max}}$

Temperature-dependent dielectric permittivity measured upto 600 °C during heating and cooling for maximum annealing temperature-dependent slow cooled KBT. Change in thermal hysteresis during heating and cooling found to be changed with increasing annealing  $T_{\max}$ .

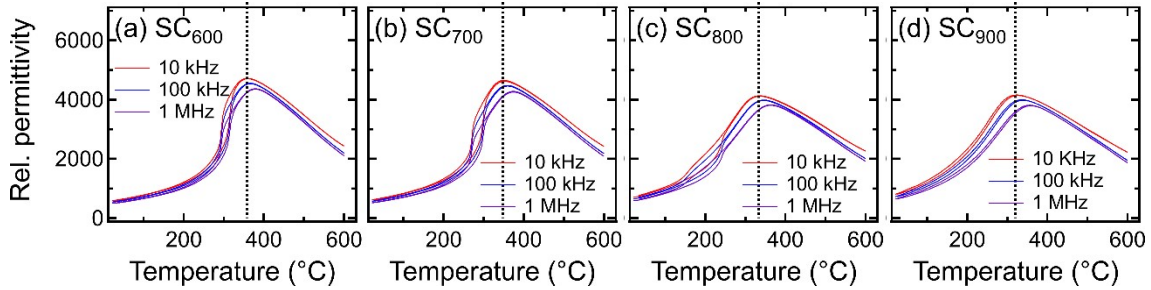


Figure S 2 Temperature-dependent dielectric permittivity of KBT samples treated with different  $T_{\max}$  with a cooling rate of 0.1 K/min.

### 3. Analysis of TF-R from dielectric permittivity data

Inverse of permittivity data<sup>[25]</sup> was used to identify the transition temperature during heating and cooling. The  $\Delta T_{F-R}$  indicates the difference in F-R and R-F transition.

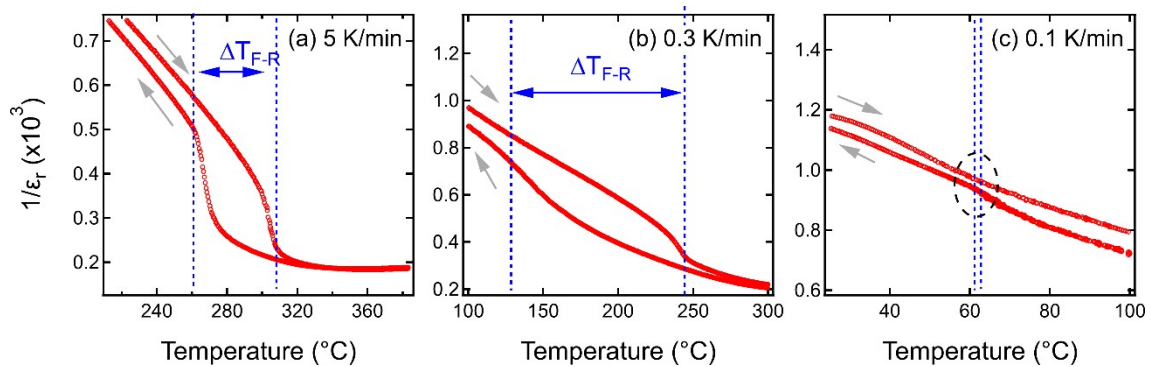


Figure S 3 Inverse dielectric permittivity for samples annealed with cooling rate (a) 5 K/min, (b) 0.3 K/min, and (c) 0.1 K/min from the  $T_{\max}$  of 900 °C

### 4. Temperature-dependent dielectric permittivity of quenched KBT from different

$T_{\max}$

Dielectric permittivity of KBT ceramics measured after quenching at different  $T_{\max}$ . A significant increase in  $T_{F-R}$  is observed for  $Q_{900}$  KBT.

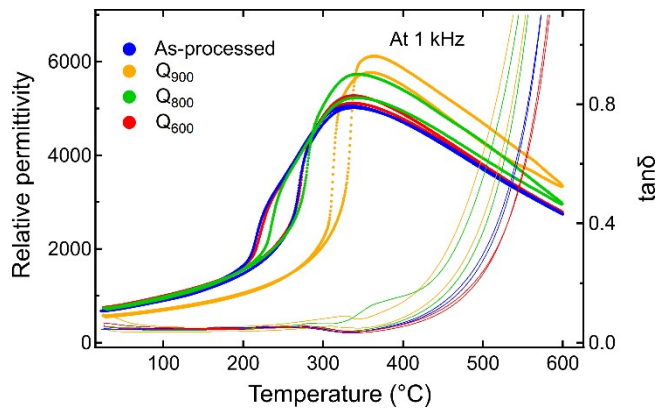


Figure S 4 Variation in dielectric permittivity for samples quenched at different  $T_{\max}$

## 5. Reversible FE-RE-FE state change in KBT

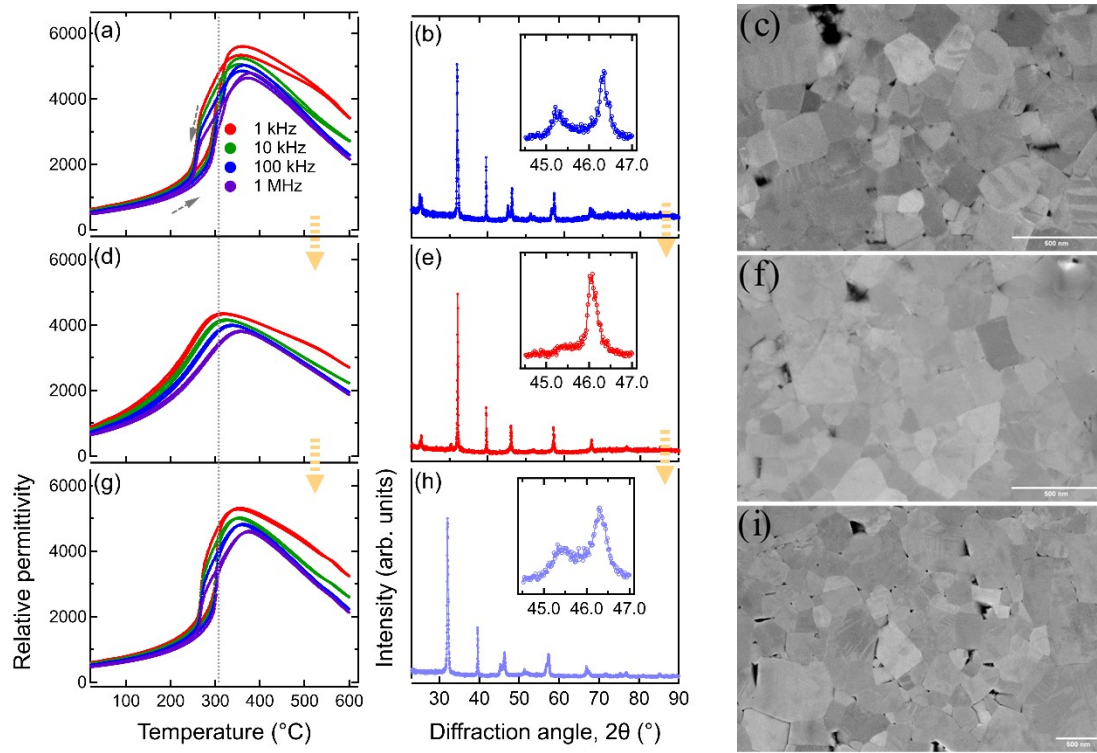


Figure S 5 Temperature-dependent permittivity, x-ray diffraction patterns, and microstructure for a single KBT sample after subsequent treatment with 5 K/min (a-c) NC<sub>900</sub>, (d-f) SC<sub>900</sub>, and (g-i) NC<sub>900</sub> indicating the slow cooling induced change can be reverted to the original state.

## 6. Simulation of NMR spectrum for TiO<sub>2</sub>

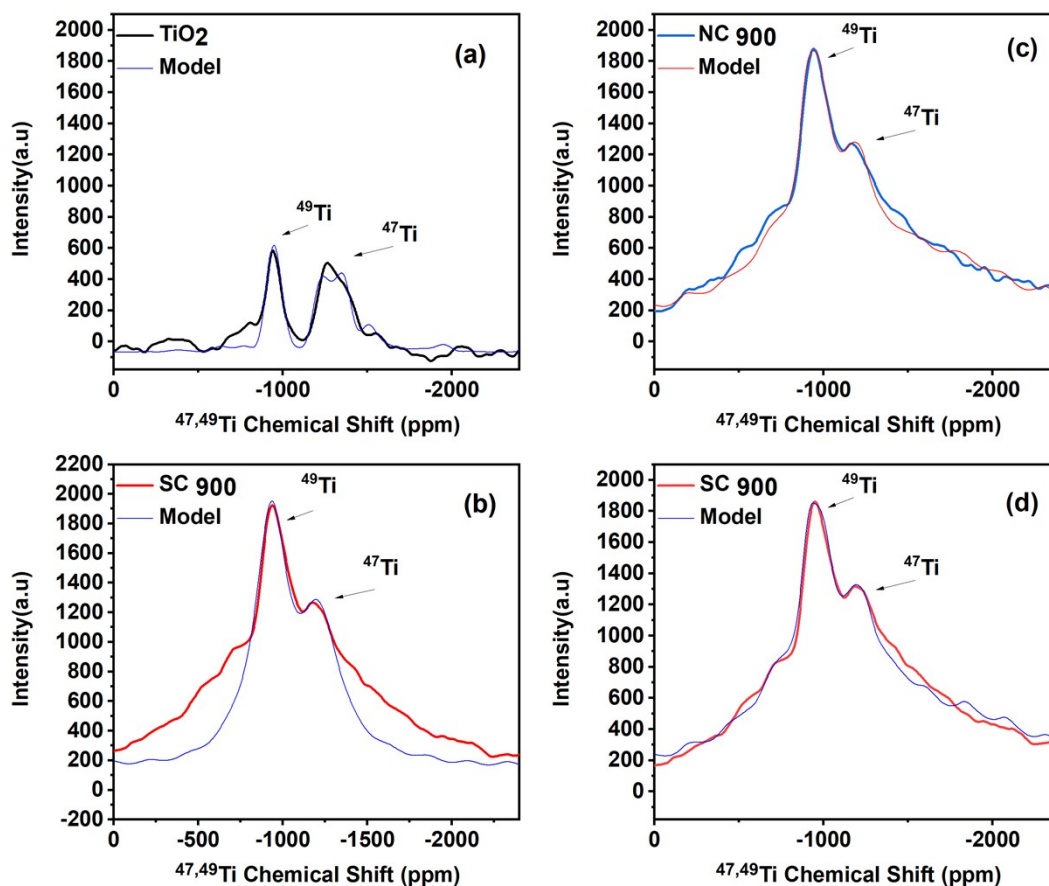


Figure S 6 Simulation of  $^{47,49}\text{Ti}$  NMR spectra with different models (a)  $\text{TiO}_2$  with int2QUAD, (b)  $\text{SC}_{900}$  KBT with int2QUAD, (c)  $\text{NC}_{900}$  KBT with Cjzek, and (d)  $\text{SC}_{900}$  KBT with Cjzek.

Simulation parameters are listed in Table S 1.

Table S 1 Simulation parameters for  $^{47,49}\text{Ti}$  NMR spectra, simulated with DMfit.<sup>[51]</sup>

	model	chemical shift (ppm)	Quadrupolar Coupling $C_Q$ (kHz)	eta	Window function (Hz)	MAS frequency (Hz)
$\text{TiO}_2$	int2QUAD	-907	4481	0	-3000	10000
$\text{NC}_{900}$	Cjzek	-870	3750* (7500)	-	3500	8000
$\text{SC}_{900}$	Cjzek	-880	4000* (8000)	-	3500	8000
$\text{SC}_{900}$	int2QUAD	-911	3122	0	8000	8000

\*average CQ value computed from the Czjzek model (value in parenthesis represents CQ\_max used as input for the distribution in dmfit) (Ref:10.1002/mrc.984)

## 7. Internal residual stress measurement using synchrotron x-ray diffraction.

The azimuth angle-dependent diffraction data were collected at the Spring8 using a monochromatic x-ray beam with an energy of 24 keV ( $\lambda = 0.5166 \text{ \AA}$ ) and with an area detector Rigaku Hypix-9000HE. A beam size of  $300 \mu\text{m} \times 300 \mu\text{m}$  was used. Azimuth angle-dependent variation in d-spacings, i.e.,  $2\theta$  position of selected individual reflections, can reveal the extent of internal residual stress in a material. Analysis of peak positions of  $110_{\text{pc}}$ ,  $111_{\text{pc}}$ , and  $200_{\text{pc}}$  reflections did not show any significant variation in internal residual stress within the sensitivity of the measurement.

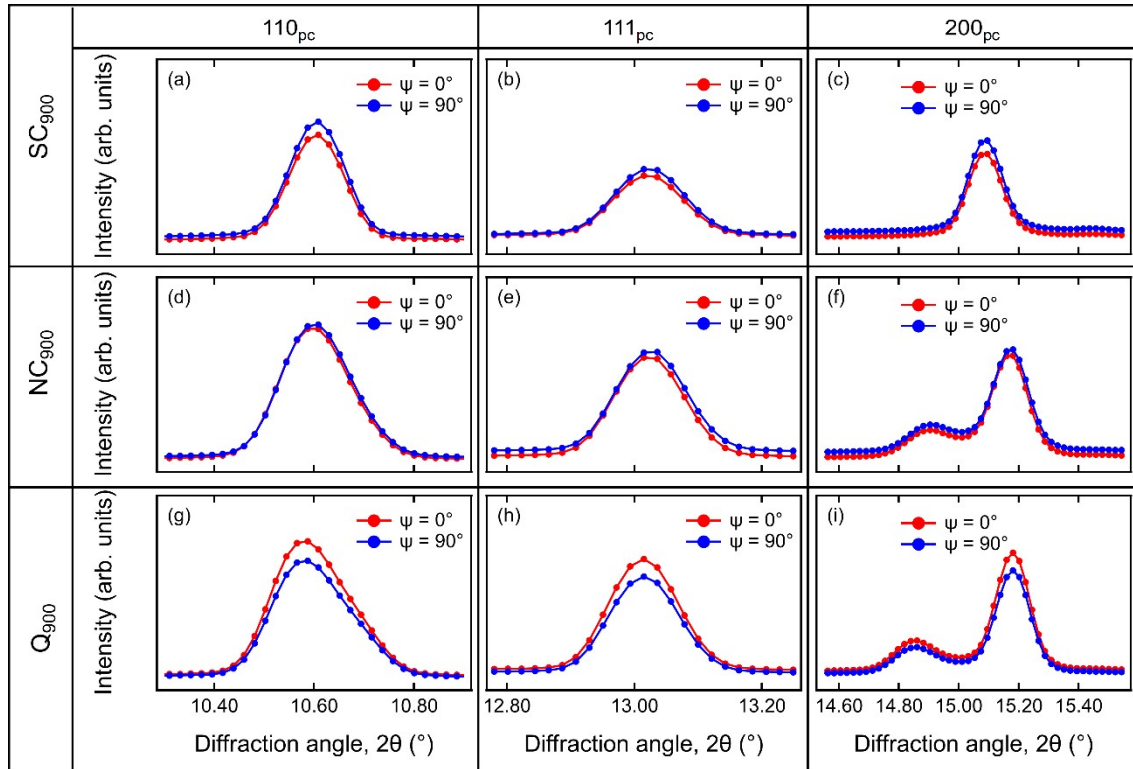


Figure S 7 Diffraction patterns of slow cooled ( $\text{SC}_{900}$ ), normal cooled ( $\text{NC}_{900}$ ), and quenched ( $\text{Q}_{900}$ ) KBT for azimuth angle,  $\psi = 0^\circ, 90^\circ$ . No significant variation in peak position with azimuth angle is evident from the diffraction data.